Elimination of Hole–Surface Overlap in Graded CdS_xSe_{1-x} Nanocrystals Revealed by Ultrafast Fluorescence Upconversion Spectroscopy

Joseph D. Keene,[†,⊥] James R. McBride,[*,†,⊥] Noah J. Orfield,[†,⊥] and Sandra J. Rosenthal[*,†,‡,§,∥,⊥,¶]

[†]Department of Chemistry, [‡]Department of Physics and Astronomy, [§]Department of Pharmacology, [∥]Department of Chemical and Biomolecular Engineering, and [⊥]The Vanderbilt Institute of Nanoscale Science and Engineering, Vanderbilt University, Nashville, Tennessee 37235, United States, and [¶]Materials Science and Technology Division, Oak Ridge National Laboratory, Oak Ridge, Tennessee 37831-6071, United States

ABSTRACT Interaction of charge carriers with the surface of semiconductor nanocrystals plays an integral role in determining the ultimate fate of the excited state. The surface contains a dynamic ensemble of trap states that can localize excited charges, preventing radiative recombination and reducing fluorescence quantum yields. Here we report quasi-type-II band alignment in graded alloy CdS_xSe_{1-x} nanocrystals revealed by femtosecond fluorescence upconversion spectroscopy. Graded alloy CdS_xSe_{1-x} quantum dots are a compositionally inhomogeneous nanoheterostructure designed to decouple the exciton from the nanocrystal surface. The large valence band offset between the CdSe-rich core and CdS-rich shell separates the excited hole from the surface by confining it to the core of the nanocrystal. The small conduction band offset, however, allows the electron to delocalize throughout the entire nanocrystal and maintain overlap with the surface. Indeed, the ultrafast charge carrier dynamics reveal that the fast 1–3 ps hole-trapping process is fully eliminated with increasing sulfur composition and the decay constant for electron trapping (~20–25 ps) shows a slight increase. These findings demonstrate progress toward highly efficient nanocrystal fluorophores that are independent of their surface chemistry to ultimately enable their incorporation into a diverse range of applications without experiencing adverse effects arising from dissimilar environments.

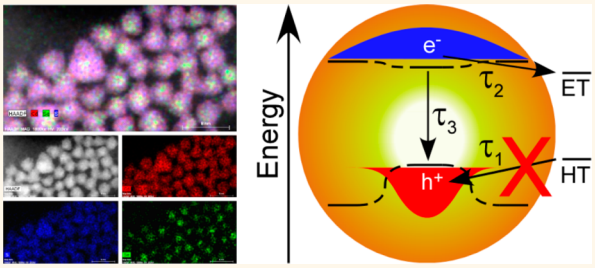

KEYWORDS: ultrafast fluorescence upconversion · nanocrystal spectroscopy · quasi-type-II · CdS_xSe_{1-x} · core/shell · graded alloy

Semiconductor nanocrystals (NCs), or quantum dots (QDs), are expansively utilized as photon sources in a wide array of applications such as light-emitting diodes, biological probes, and low threshold lasers due to their (potentially) high photoluminescence quantum yields (PLQYs) and their size-dependent optoelectronic properties arising from quantum confinement.[1−5] The NC surface, however, has long been implicated as a source of trap states that localize excited charge carriers and inhibit radiative recombination of the electron and hole. Early studies yielded efforts to promote passivation of the NC surface with various organic ligands, such as hexadecylamine and trioctylphosphine oxide, as cosurfactants to reduce the number of trap sites and moderate carrier trapping.[6−8] More recent work suggests that NC surface atoms are in a state of dynamic flux under excitation, resulting in an ever-changing population of surface and subsurface states available to localize charge carriers.[9,10] This revelation of a fluxional surface suggests that decoupling the exciton from the NC surface, as opposed to the long-held notion of passivating the NC surface, is essential for optimal enhancement of the photophysical properties of semiconductor NCs. The obvious response to this discovery comes in the form of type-I or quasi-type-II core/shell NC heterostructures wherein a NC is encapsulated in a semiconductor shell of wider band gap to confine either both (type-I, Figure 1a) or a single (quasi-type-II, Figure 1b) charge carrier to the core and minimize their surface overlap.[11] Aberration-corrected atomic number scanning transmission electron microscopy (Z-STEM) was performed on CdSe/ZnS and CdSe/CdS core/shell

* Address correspondence to james.r.mcbride@vanderbilt.edu, sandra.j.rosenthal@vanderbilt.edu.

Received for review July 30, 2014 and accepted September 9, 2014.

Published online September 09, 2014
10.1021/nn504235w

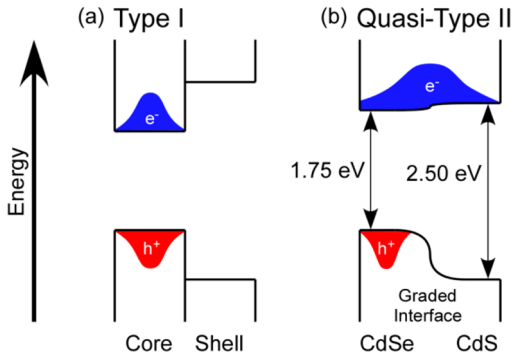

Figure 1. Type-I (a) and quasi-type-II (b) electronic band alignments illustrating that both carriers are confined to a single material in type-I and only a single carrier is confined in quasi-type-II. Shown in (b) is the electronic band alignment between zinc blende CdSe and CdS[15] and the relaxed confinement potential afforded by a graded alloy interface between the materials.

NCs and showed that complete shell coverage is necessary to achieving PLQYs near unity; however, current shell growth techniques such as successive ion layer adsorption and reaction (SILAR) yield preferential growth on anion-terminated facets.[12] Due to nonuniform faceted shell growth, upward of 18 monolayers of material are needed for complete shell coverage, yielding large and bulky NCs often exceeding 20 nm in diameter that can require days to synthesize and are not ideal in some biological imaging applications.[13] Additionally, the abrupt boundary between core and shell materials can induce strain due to lattice mismatch and introduce new trap states at the interface.[14] McBride *et al.* ultimately concluded that a graded shell is necessary for complete coverage of the semiconductor NC core.[12] The full surface coverage and passivation afforded by the graded shell, as opposed to "patchy" shells often obtained with a hard interface, are predicted to more effectively confine charge carriers away from the surface of the nanocrystal and provide optimal enhancement of the fluorescence properties.[12]

In addition to maximum coverage with a graded shell, the gradual transition from the core to the shell materials also relaxes the confinement potential at the interface by providing an intermediate area of chemical composition which, as illustrated in Figure 1b, is correspondingly reflected in the band structure of the NC.[15] Investigations of graded type-I and quasi-type-II core/shell NCs have established improvement over nongraded core/shell QDs. The relaxed confinement potential afforded by the graded shell structure and the accompanying suppression of Auger processes inhibit single NC fluorescence intermittency and improve the multiexciton performance of QDs.[16,17] Theory and experiment have shown that the rate of nonradiative Auger recombination governs biexciton decay and is driven by the interfacial properties of the QD.[15,18,19] However, the effect of the confinement potential gradient in the context of charge carrier interaction with the NC surface has been largely unexplored. Extensive ultrafast dynamics studies detailing charge carrier overlap with the NC surface of binary semiconductor NCs have revealed that charge trapping at the surface is very sensitive to NC size and can be readily tuned *via* modification of the NC surface chemistry.[6−8,20−23] Furthermore, homogeneous CdS_xSe_{1-x} alloys were found to have trapping kinetics that were also dependent on chemical composition with charge trapping dominating the exciton decay processes as sulfur content increased.[24] Here, femtosecond fluorescence upconversion spectroscopy is utilized to investigate the ultrafast dynamics of graded alloy CdS_xSe_{1-x} semiconductor NCs to probe the chemical composition dependence of charge carrier trapping at the NC surface of graded alloy CdS_xSe_{1-x} nano-heterostructures. We observe complete isolation of the excited hole from the NC surface and trapping kinetics that are dictated by the surface chemistry of the QDs.

RESULTS AND DISCUSSION

Compositionally graded alloy CdS_xSe_{1-x} NCs were synthesized according to procedure developed by Harrison *et al.* based on differing reactivities of the anionic precursors (see Materials and Methods).[25] These NCs have been thoroughly characterized in previous literature,[25] and comprehensive optical (absorption, fluorescence) and structural (HRTEM, EDS) characterization of these graded alloy CdS_xSe_{1-x} NCs is included in the Supporting Information. Briefly, optical absorption of the structural evolution of a representative compositionally graded CdS_xSe_{1-x} sample (Figure 2a) reveals an initial spectrum consistent with that of CdSe NCs, displays a slight red shift as the sample evolves during the synthesis, and eventually stagnates before the synthesis is terminated. Additionally, the final graded alloy CdS_xSe_{1-x} structures (Figure 2b) exhibit a blue shift with an increase in sulfur composition, indicating a higher degree of quantum confinement. The size and morphology of the NCs were determined *via* high-resolution transmission electron microscopy (HRTEM), and in accord with the previous reported synthesis of these nanoparticles,[25] the NCs exhibit slight growth throughout the synthesis after initial core formation (Figure 2c) even while S/(S+Se) ratios are observed to change. The optical and electron microscopy results can be explained by partial anion exchange of surface or near-surface selenium with the excess sulfur in the reaction mixture after growth has stopped.[26] Additionally, the final structures are similar in size for all chemical compositions (Figure 2d); because the ultrafast dynamics of semiconductor NC carriers are very sensitive to size,[6] similar NC diameters permit direct comparison analyses of the carrier-trapping kinetics.

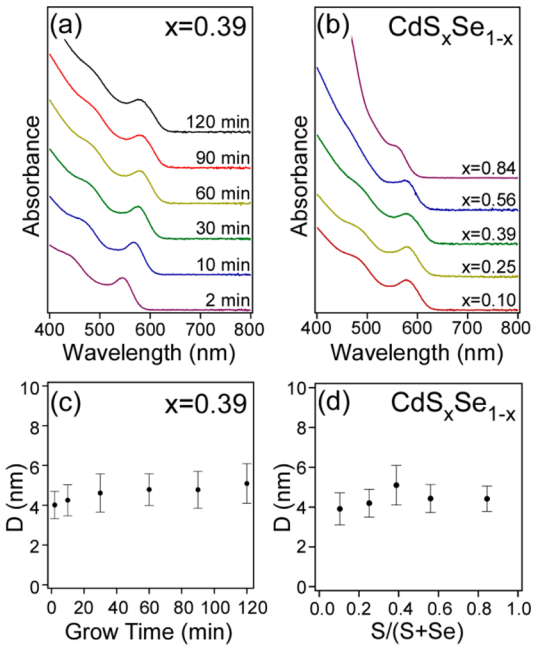

Figure 2. Optical absorption (a) and diameters (c) of aliquots taken during the structural evolution of $CdS_{0.39}Se_{0.61}$ (1:1 S/Se anion injection ratio). Optical absorption (b) and diameters (d) of the final graded CdS_xSe_{1-x} structures (120 min aliquots). The graded alloy diameters are comparable for all samples, while the blue shift in absorbance for higher sulfur compositions (b) indicates greater confinement of the charge carrier(s).

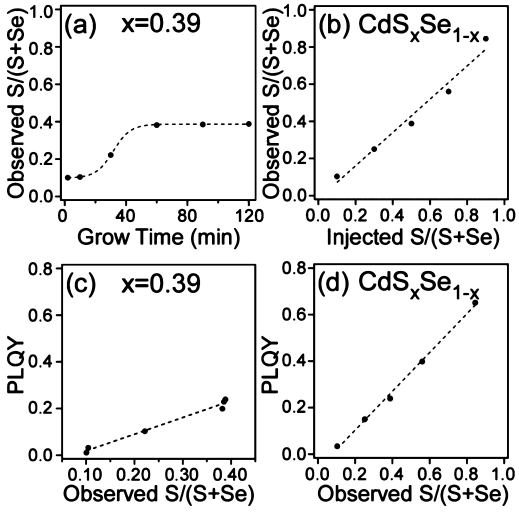

Figure 3. Chemical composition (a) and PLQY (c) of aliquots taken from the 1:1 S/Se anion injection synthesis. Observed *versus* injected sulfur compositions (b). The PLQY of the final graded CdS_xSe_{1-x} structures as a function of chemical composition (d). The nonlinear increase in chemical composition with growth time (a) demonstrates the inhomogeneity of the sulfur incorporation into the nanocrystals. The PLQY is directly related to the chemical composition of the graded alloys (c,d).

In order to determine the chemical composition of the NCs, energy-dispersive X-ray spectroscopy (EDS) was performed on each aliquot after rigorous purification (see Materials and Methods). Figure 3a displays the chemical composition for a representative graded alloy synthesis and shows a nonlinear increase in sulfur composition with growth time, which confirms the graded inhomogeneity of the NC structure. This is in direct contrast to homogeneous alloys which maintain constant chemical composition with growth time.[27] Additionally, the sulfur composition of the final graded structures corresponds to the initial anion injection ratios (Figure 3b). The PLQY of the graded alloy NCs increases with sulfur composition both as the NC structure evolves during each synthesis (Figure 3c) and for the final graded alloy NCs (Figure 3d). PLQY values up to 65% are reported here for $CdS_{0.84}Se_{0.16}$ graded alloy NCs. Finally, EDS scanning TEM was performed on $CdS_{0.84}Se_{0.16}$ NCs for further verification of the graded alloy structure. As seen in Figure 4, cadmium is evenly distributed throughout the NCs while the sulfur-rich shell extends beyond the selenium-rich core.

The carrier dynamics of the graded alloy CdS_xSe_{1-x} NCs were probed with femtosecond fluorescence upconversion spectroscopy. The laser system has been previously described[8,24] (see Materials and Methods). Since this technique only monitors radiative recombination of the exciton, any carrier trapping at the NC surface is realized as a decrease in the fluorescence intensity. The ultrafast fluorescence upconversion spectra for the CdS_xSe_{1-x} NCs are displayed in Figure 5. The same trend was observed for the evolution of CdS_xSe_{1-x} NCs for each S/Se anion injection ratio as for the final graded alloy CdS_xSe_{1-x} NCs: an increase in sulfur composition yields a decrease in charge carrier trapping, as evidenced by a less pronounced decay of the fluorescence intensity as a function of time (Figure 5). Due to the similar behavior, we present the analysis of the final graded alloy structures (120 min aliquots) in this article, and the results are analogous for the structural evolution of each sample as sulfur is incorporated into the NCs (included in the Supporting Information). Interestingly, graded alloy CdS_xSe_{1-x} NCs of low sulfur content (S/(S+Se) < 0.34) display triple exponential decay behavior, whereas NCs with higher sulfur composition exhibit double exponential decay behavior. Historically, unpassivated and under-coordinated surface anions have been implicated as midgap states that are available as "dangling bonds" to trap holes in CdSe NCs within the first few picoseconds after excitation.[22,23] Previous work on CdS NCs attribute a fast 2−3 ps decay to hole trapping at the surface based on a higher density of hole-trapping states near the valence band (VB) due to its larger effective mass.[28,29] However, taking into account the recent proposal of a dynamic nanocrystal surface under excitation, under-coordinated and unpassivated anions exist within ~1 nm of the surface of the nanocrystal due to the fluxionality of those atoms; that is, instead of a crystalline, faceted lattice at the surface, the atoms are in motion and thus are not fully passivated at

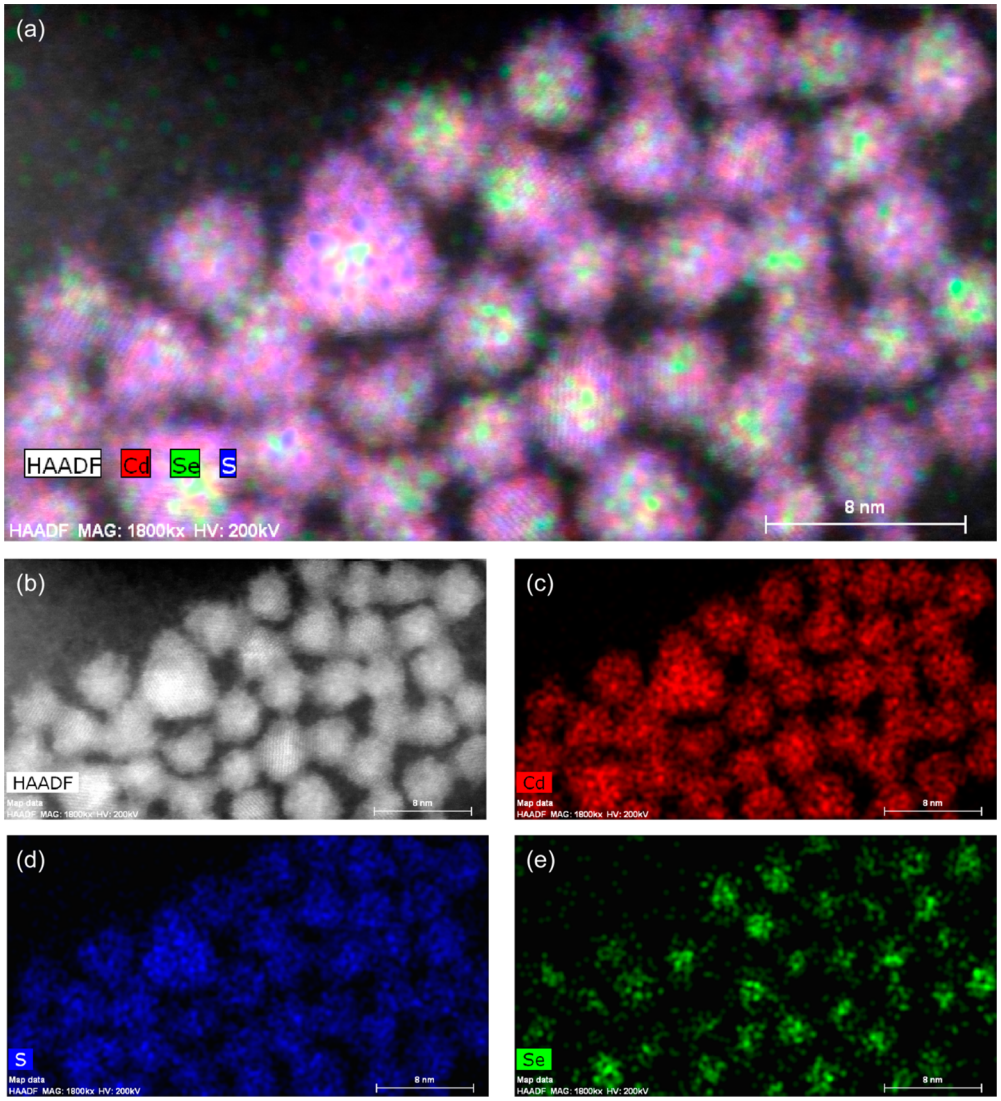

Figure 4. Superposition (a) of the high-angle annular dark-field image (b) and EDS maps of cadmium (c), sulfur (d), and selenium (e) for graded alloy $CdS_{0.84}Se_{0.16}$ NCs. Scale bars are 8 nm. The cadmium is evenly distributed throughout the NCs, while the sulfur-rich shell extends beyond the selenium-rich core.

any given moment, increasing the likelihood of their availability to act as a hole trap. We report decay constants for the first exponential decay (τ_1) of ~3 ps (Figure 6a), in good agreement with the literature for hole trapping in CdSe and CdS NCs. The τ_1 decay constant is consistent for all CdS_xSe_{1-x} NCs; however, the first decay becomes less prevalent up to a sulfur composition of ~34%, as indicated by a decrease in τ_1 amplitude (Figure 6d), at which point the decay completely disappears from the ultrafast fluorescence upconversion data. This is direct evidence for the quasi-type-II band structure alignment created by the CdS-rich shell encapsulating the CdSe-rich core which, based on the VB offset between the materials, functions as a "hole well" in which the hole is confined to the core of the NC heterostructure. Elimination of the fast hole-trapping process from the carrier dynamics demonstrates successful separation of the hole from within ~1 nm of the NC surface and confirms the proposed graded alloy structure.

The second exponential decay process in the graded alloy CdS_xSe_{1-x} NCs was found to have a decay constant of 20−25 ps, increasing with sulfur composition (Figure 5b). Electron trapping in CdSe NCs is a process that occurs tens to hundreds of picoseconds after excitation[22,23] and has been reported as a 20−30 ps decay in CdS NCs.[28,29] Our results for τ_2 are in good agreement with the reported literature values for electron trapping in CdSe and CdS NCs. This supports the quasi-type-II band structure of the graded alloy CdS_xSe_{1-x} NCs in which the excess electron energy in the conduction band (CB) is greater than the confinement potential of the CB offset of only ~0−0.1 eV between the CdSe-rich core and the CdS-rich shell.[15,30] Therefore, the electron is delocalized throughout both the core and shell materials and maintains access to

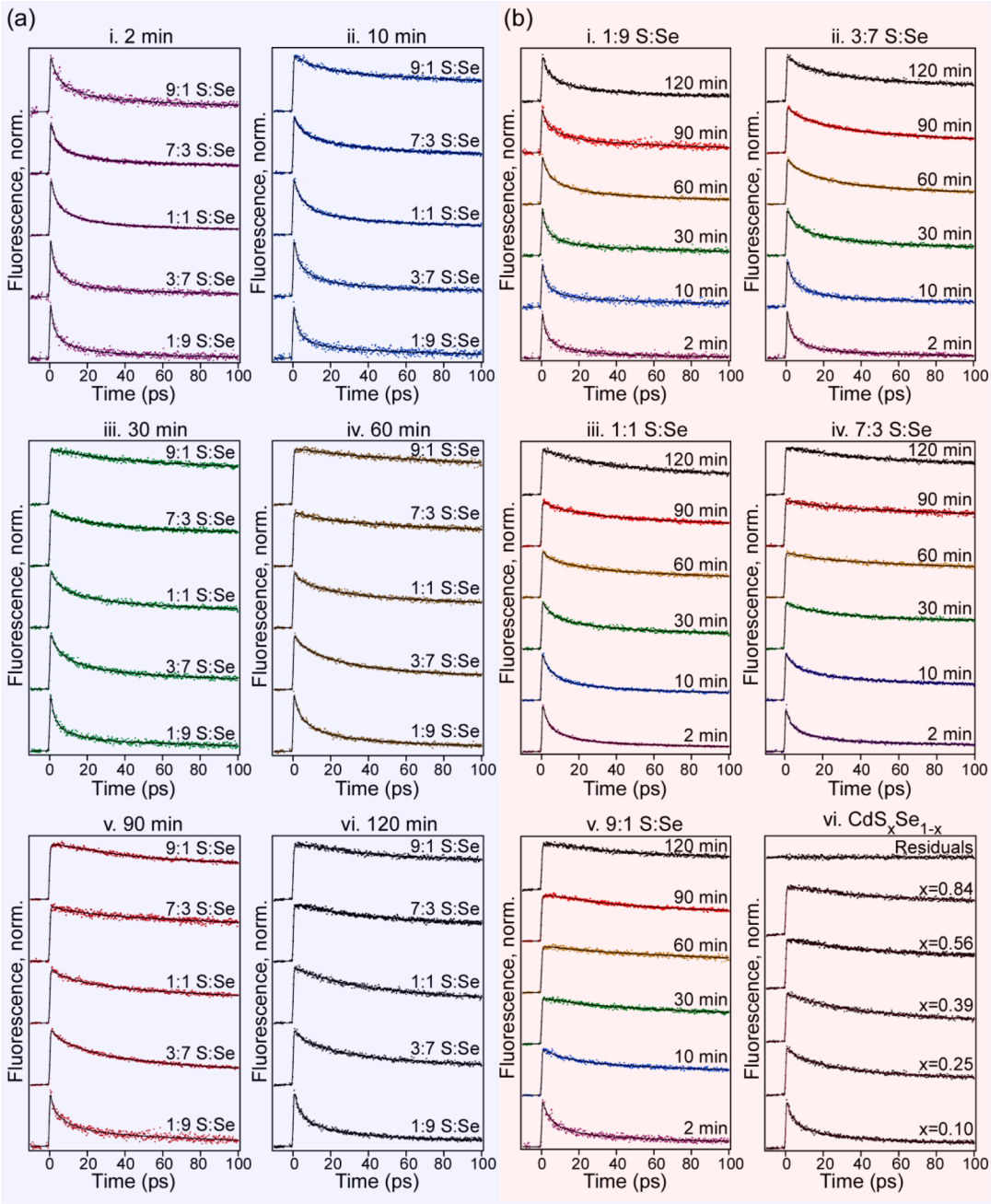

Figure 5. Ultrafast fluorescence upconversion spectra of graded alloy CdS_xSe_{1-x} NCs. Carrier trapping is observed indirectly as a fast decay of the fluorescence intensity. The spectra are plotted according to (a) reaction time points and (b) S/Se injection ratios to show the reduced trapping as sulfur is more quickly incorporated into the alloys with higher S/Se injection ratios and as the graded alloy NC structures evolve during each S/Se injection ratio synthesis, respectively. The top trace in (b-vi) is the plotted residuals for graded $CdS_{0.25}Se_{0.75}$ NCs (x = 0.25) and is representative of all fits. All samples were excited at 50 nm above the band gap and observed at the wavelength corresponding to maximum fluorescence intensity.

the NC surface for all sulfur compositions. Indeed, the 20−25 ps electron trapping is present in all CdS_xSe_{1-x} NCs regardless of sulfur composition. Traditionally, the surface of NCs has been envisioned as a static crystalline interface that may contain cadmium adatoms and/or cadmium atoms that are not fully coordinated or passivated and therefore are available to trap electrons. However, according to the recent proposal of a fluxional NC surface under excitation, the atoms within ~1 nm of the surface are physically in motion at any given moment as part of a dynamic noncrystalline "lattice" at the NC surface interface; thus, there exists an ever-changing population of cadmium atoms that, similar to what has been proposed for the static surface, are potentially under-coordinated and therefore are available as electron trap states.

Finally, the third exponential decay process corresponds to radiative relaxation of the exciton. Excited

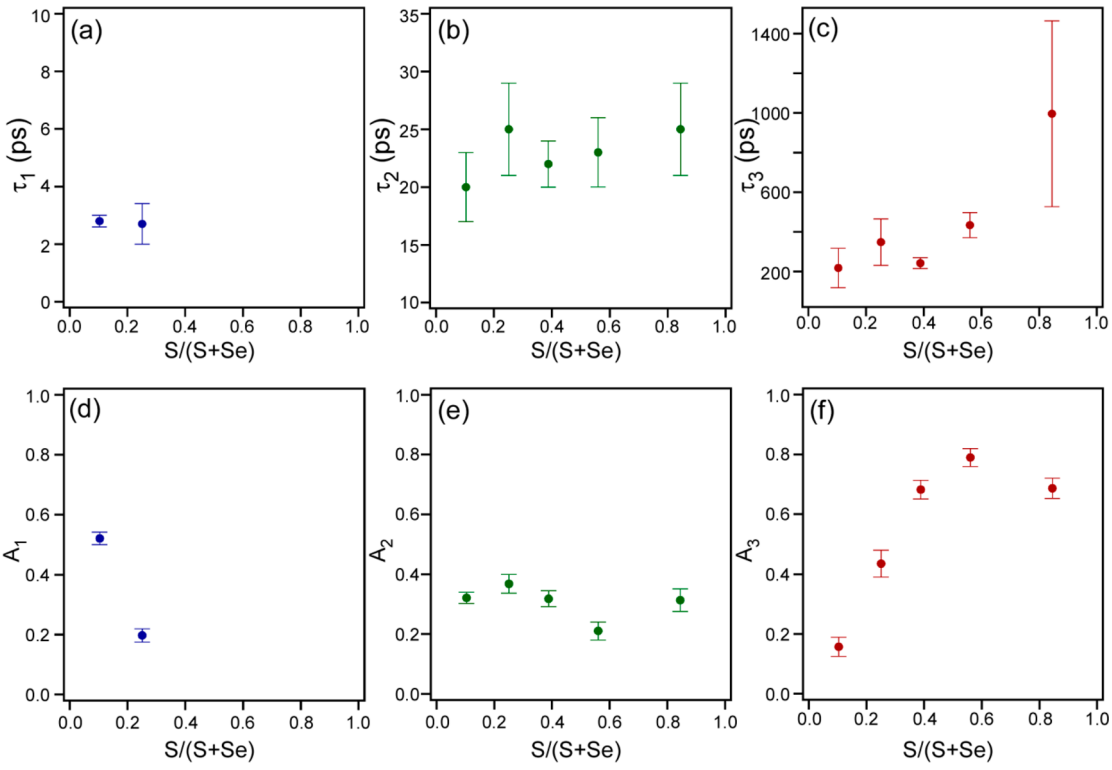

Figure 6. Exponential decay constants τ_1 (a), τ_2 (b), and τ_3 (c) and the corresponding amplitudes A_1 (d), A_2 (e), and A_3 (f) for the final graded CdS_xSe_{1-x} NCs as a function of sulfur composition. As sulfur composition increases, hole trapping (τ_1) is eliminated, the electron-trapping decay constant (τ_2) increases, and exciton lifetime decay constant (τ_3) increases, all indicative of reduced carrier interaction (trapping) with (at) the nanocrystal surface.

electron−hole pair recombination in semiconductor NCs is a nanosecond process[22,23] and extends beyond the capabilities of our upconversion experiment (100 ps). Therefore, the τ_3 time constants reported from our analysis of the ultrafast fluorescence decay curves do not represent actual measured lifetime values for the radiative relaxation of the exciton; however, they allow our model to decay to baseline as determined by y_0 before the excitation pulse arrives.[31,32] Nevertheless, a clear trend of an increase in τ_3 is observed as sulfur content increases (Figure 6c), indicating longer lifetimes. Notably, the first and third decay amplitudes are inversely related; as the first decay disappears, the third decay increases and begins to dominate the exciton decay processes (Figure 6d,f). This is exactly the opposite behavior reported for the charge carrier dynamics of homogeneous alloy CdS_xSe_{1-x} NCs where the first decay amplitude increases and carrier trapping begins to dominate with an increase in sulfur composition.[24] These findings afford further validation of the inhomogeneous chemical composition of the graded alloy CdS_xSe_{1-x} NCs.

By focusing on the first few picoseconds after the arrival of the excitation pulse, we also investigated the initial population of the band edge radiative states, $1S_{3/2}$ and $1S_e$ for the VB and CB, respectively.[33] Figure 7a displays a representative fluorescence upconversion spectrum of a CdS_xSe_{1-x} sample as the pulse arrives

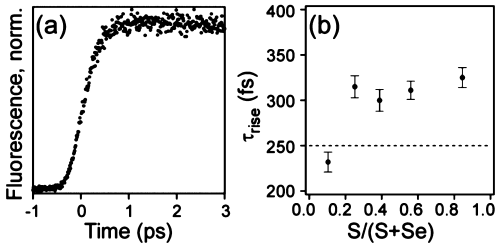

Figure 7. Ultrafast fluorescence upconversion spectrum of $CdS_{0.39}Se_{0.61}$ (a) and observed rise times (τ_{rise}) as a function of sulfur composition (b). Subpicosecond rise times exhibit a slight increase with sulfur composition and correspond to hot hole cooling in the valence band. The sample was excited at 50 nm above band gap (530 nm) and observed at the maximum fluorescence intensity (604 nm). Note: The dotted line in (b) indicates the instrument resolution.

and an electron is promoted from the VB to the CB. The data were fit with an additional exponential decay, albeit with a negative amplitude, in order to determine if a rise time (τ_{rise}) is present. Since only the band edge radiative recombination is observed in these experiments, a rise time represents the temporal delay between excitation of the charge carriers and the onset of emission by the NC. Since we excited the samples 50 nm above the band gap, the $1S_e$ state in the CB was initially populated with an electron from the $2S_{3/2}$ state in the VB.[34,35] Therefore, the hole in the $2S_{3/2}$ state must undergo intraband cooling/relaxation to the $1S_{3/2}$ state

before band edge radiative recombination can occur; this delay is realized as a rise time in the temporal fluorescence upconversion spectra. As seen in Figure 7b, the observed rise times are at or slightly longer than the pulse width, which defines the temporal resolution of the experiment (see Materials and Methods), and are consistent with values reported for intraband hole cooling in CdSe NCs.[6,36] We do note a slight additional rise of 8−10 ps for the highest sulfur compositions (S/(S+Se) > 0.5), and additional studies are ongoing to probe the excitation- and emission-dependent dynamics of the graded alloy $CdS_{0.84}Se_{0.16}$ NCs. These studies on the graded structure with the highest sulfur content that most prominently exhibits quasi-type-II behavior are expected to provide additional insight into the relationship between the core/shell interface and the surface interaction of excited charge carriers.

Our results and analyses of the ultrafast dynamics of graded alloy CdS_xSe_{1-x} NCs highlight the importance of charge carrier interaction with the surface of semiconductor NCs. However, the carrier dynamics also show a clear structural chemical composition dependence that affects the *magnitude* of trapping and can even eliminate carrier (hole) overlap with the NC surface through proper electronic band gap engineering of the core and shell materials. This is evidenced by the disappearance of hole trapping in graded alloy CdS_xSe_{1-x} as sulfur is incorporated into the structure and the VB offset becomes great enough to confine the hole to the core of the NC and eliminate the interaction of the hole with the surface. However, for any charge carriers that do overlap with the NC surface, it is clear that the chemical composition of the NC surface, as opposed to the internal NC architecture, is what determines the *behavior* of the charge carrier trapping. Even though the graded alloy CdS_xSe_{1-x} NCs have predominantly CdSe-rich cores, the ultrafast carrier-trapping processes most closely resemble those of charge carriers in CdS NCs which exhibit fast 2−3 ps hole-trapping and longer 20−30 ps electron-trapping kinetics because the surface composition of the NCs most closely resembles CdS. Notably, it is this interplay between the internal structure and the chemical composition of the surface that ultimately determines the fate of the exciton in quantum confined nanostructures.

CONCLUSIONS

We have presented direct time-resolved spectroscopic evidence for quasi-type-II band alignment in graded alloy CdS_xSe_{1-x} NCs through analysis of the ultrafast charge carrier dynamics as a function of chemical composition. The fast ~3 ps hole-trapping process disappears as sulfur composition increases to form a graded CdS-rich shell with VB offset such that excited holes are confined to the CdSe-rich core. These results demonstrate that charge (hole) carrier interaction with the surface can be completely eliminated in NC structures with dimensions less than 5 nm, a phenomenon that typically requires a "giant" core/shell heterostructure. The 20−25 ps electron trapping is consistent in amplitude throughout all sulfur compositions in the graded alloy CdS_xSe_{1-x} NCs, with a slight increase in τ_2 decay constant with sulfur composition. Our findings demonstrate progress toward highly efficient nanocrystal fluorophores that are independent of their surface chemistry to enable their incorporation into a diverse range of applications without experiencing adverse effects arising from dissimilar environments.

MATERIALS AND METHODS

Cadmium oxide (CdO), 1-octadecene (ODE, 90%), oleic acid (OA, 90%) and tri-*n*-butylphosphine oxide (TBP, 93%) were purchased from Sigma-Adrich. Elemental selenium (Se, 99.99%) was purchased from Strem, and sulfur powder (USP sublimed) was purchased from Fisher Scientific. All reagents were used as-purchased without further purification.

Compositionally graded alloy CdS_xSe_{1-x} NCs were synthesized according to procedure developed by Harrison *et al.*[25] Briefly, 1 mmol CdO, 4 mmol OA, and 20 mL of ODE were loaded into a 250 mL three-neck round-bottom flask and heated to 220 °C under ultrahigh purity (UHP) Ar. Once the reaction solution was clear and colorless, a mixed solution of 0.8*x* mL 0.75 M Se/TBP and 0.8(1−*x*) mL of 0.75 M S/TBP was injected to the flask. Nanocrystals were grown for 2 h, and sample aliquots were pulled from the reaction vessel at 2, 10, 30, 60, 90, and 120 min for S/Se anion injection ratios of 1:9, 3:7, 1:1, 7:3, and 9:1. Aliquots were quenched with a mixture of butanol and ethanol and precipitated *via* centrifugation. Further cleaning was carried out by solvating in toluene and subsequent precipitation with ethanol *via* centrifugation; the cleaning step was repeated once. The nanocrystals were suspended in deoxygenated anhydrous toluene for ultrafast fluorescence upconversion spectroscopy measurements.

Absorption spectra were obtained using a Varian Cary 50 UV−vis spectrophotometer. Photoluminescence spectra were obtained using a Photon Technology International QuantaMaster 40. Photoluminescence quantum yields of the CdS_xSe_{1-x} in toluene were obtained using the single-point method[37] using coumarin 153 in ethanol (Q = 0.38),[38] Rhodamine 6G in methanol (Q = 0.94),[39] or sulforhodamine B in ethanol (Q = 0.69)[40] dyes as reference fluorophores, choosing the dye with optical absorption and fluorescence spectra that overlap those of the NC samples. High-resolution transmission electron microscopy (HR-TEM), energy-dispersive X-ray spectroscopy (EDS), and EDS scanning TEM were obtained using a FEI Tecnai Osiris.

Femtosecond fluorescence upconversion spectroscopy was performed with a laser system previously described[8,24] with modifications. Briefly, a Coherent Verdi V18 (CW, 532 nm, 18 W) pumped a mode-locked Ti:sapphire oscillator (Mira 900 Basic, Coherent) which then seeded a regenerative amplifier (RegA 9000, Coherent). The RegA powered an optical parametric amplifier (OPA 9400, Coherent), from which the excitation (wavelength tunable, 450−700 nm) and gate (800 nm) pulses were extracted. The system operated at 250 kHz and produced pulses ~200 fs, leading to instrument response functions (IRFs) <250 fs. Samples were pumped at 50 nm higher in energy than band edge absorption to eliminate upconversion of scattered pump photons in the upconverted fluorescence spectra. Samples were of optical density, ~0.9 (always <1), at pump energy and were stirred under UHP Ar in a 2 mm cuvette to avoid

buildup of photocharged dots. A rhodium-coated elliptical reflector focused sample emission onto a nonlinear crystal (1 mm XC8-$LiIO_3$-type-I SFM-800/500-1000//308-444 nm, Cleveland Crystals, Inc.). A UV-dispersing prism (STS#37261, CVI Laser Corp.) separated upconverted signal from any residual photons. The signal was directed into a UV-optimized monochromator (McPherson), detected by a photon-counting photomultiplier tube (R1527P, Hamamatsu) and digitized with a photon counter (SR400, Stanford Research Systems). The fitting function used to analyze the data was derived from the convolution of the Gaussian laser pulse with a decaying exponential,[41] with the addition of a time shift (t_0) to allow the Gaussian to float relative to the exponentials and an offset (y_0) so the exponentials decay to baseline instead of zero:

$$Fit = \sum_{i=0}^{n}\left[\frac{A_i}{2}\left(1+erf\left[\left(\frac{1}{4}\right)\frac{8(t-t_0)(\ln 2)-W^2/\tau_i}{W\sqrt{\ln 2}}\right]\right)\exp\left[\frac{-(16(t-t_0)(\ln 2)/\tau_i)-W^2/{\tau_i}^2}{16\ln 2}\right]\right]+y_0 \quad (1)$$

where A_i is the ith decay amplitude, W is fwhm of the Gaussian IRF, and τ_i is the ith decay time. The fit function is the summation of as many convolved functions as observed decay processes.

Conflict of Interest: The authors declare no competing financial interest.

Acknowledgment. J.D.K. and N.J.O. were supported by the National Science Foundation (CHE-1213758). HRTEM and EDS-STEM images were acquired using an FEI Tecnai Osiris electron microscope supported by the National Science Foundation (EPS-1004083).

Supporting Information Available: Static optical (absorption, fluorescence) and structural (HRTEM, EDS) characterization of graded CdS_xSe_{1-x} NCs. Notes on ultrafast fluorescence upconversion data analysis. Ultrafast decay constants and amplitudes for all CdS_xSe_{1-x} samples. This material is available free of charge *via* the Internet at http://pubs.acs.org.

REFERENCES AND NOTES

1. Schreuder, M. A.; Xiao, K.; Ivanov, I. N.; Weiss, S. M.; Rosenthal, S. J. White Light-Emitting Diodes Based on Ultrasmall CdSe Nanocrystal Electroluminescence. *Nano Lett.* **2010**, *10*, 573–576.
2. Klimov, V. I.; Mikhailovsky, A. A.; Xu, S.; Malko, A.; Hollingsworth, J. A.; Leatherdale, C. A.; Eisler, H. J.; Bawendi, M. G. Optical Gain and Stimulated Emission in Nanocrystal Quantum Dots. *Science* **2000**, *290*, 314–317.
3. Bruchez, M.; Moronne, M.; Gin, P.; Weiss, S.; Alivisatos, A. P. Semiconductor Nanocrystals as Fluorescent Biological Labels. *Science* **1998**, *281*, 2013–2016.
4. Schreuder, M. A.; Gosnell, J. D.; Smith, N. J.; Warnement, M. R.; Weiss, S. M.; Rosenthal, S. J. Encapsulated White-Light CdSe Nanocrystals as Nanophosphors for Solid-State Lighting. *J. Mater. Chem.* **2008**, *18*, 970–975.
5. Rosenthal, S. J.; Chang, J. C.; Kovtun, O.; McBride, J. R.; Tomlinson, I. D. Biocompatible Quantum Dots for Biological Applications. *Chem. Biol.* **2011**, *18*, 10–24.
6. Underwood, D. F.; Kippeny, T.; Rosenthal, S. J. Ultrafast Carrier Dynamics in CdSe Nanocrystals Determined by Femtosecond Fluorescence Upconversion Spectroscopy. *J. Phys. Chem. B* **2001**, *105*, 436–443.
7. Kippeny, T. C.; Bowers, M. J.; Dukes, A. D.; McBride, J. R.; Orndorff, R. L.; Garrett, M. D.; Rosenthal, S. J. Effects of Surface Passivation on the Exciton Dynamics of CdSe Nanocrystals As Observed by Ultrafast Fluorescence Upconversion Spectroscopy. *J. Chem. Phys.* **2008**, *128*, 084713.
8. Garrett, M. D.; Bowers, M. J.; McBride, J. R.; Orndorff, R. L.; Pennycook, S. J.; Rosenthal, S. J. Band Edge Dynamics in CdSe Nanocrystals Observed by Ultrafast Fluorescence Upconversion. *J. Phys. Chem. C* **2008**, *112*, 436–442.
9. Pennycook, T. J.; McBride, J. R.; Rosenthal, S. J.; Pennycook, S. J.; Pantelides, S. T. Dynamic Fluctuations in Ultrasmall Nanocrystals Induce White Light Emission. *Nano Lett.* **2012**, *12*, 3038–3042.
10. McBride, J. R.; Pennycook, T. J.; Pennycook, S. J.; Rosenthal, S. J. The Possibility and Implications of Dynamic Nanoparticle Surfaces. *ACS Nano* **2013**, *7*, 8358–8365.
11. Kim, S.; Fisher, B.; Eisler, H. J.; Bawendi, M. Type-II Quantum Dots: CdTe/CdSe(core/shell) and CdSe/ZnTe(core/shell) Heterostructures. *J. Am. Chem. Soc.* **2003**, *125*, 11466–11467.
12. McBride, J.; Treadway, J.; Feldman, L. C.; Pennycook, S. J.; Rosenthal, S. J. Structural Basis for Near Unity Quantum Yield Core/Shell Nanostructures. *Nano Lett.* **2006**, *6*, 1496–1501.
13. Chen, Y.; Vela, J.; Htoon, H.; Casson, J. L.; Werder, D. J.; Bussian, D. A.; Klimov, V. I.; Hollingsworth, J. A. "Giant" Multishell CdSe Nanocrystal Quantum Dots with Suppressed Blinking. *J. Am. Chem. Soc.* **2008**, *130*, 5026–5027.
14. Dabbousi, B. O.; Rodriguez-Viejo, J.; Mikulec, F. V.; Heine, J. R.; Mattoussi, H.; Ober, R.; Jensen, K. F.; Bawendi, M. G. (CdSe)ZnS Core−Shell Quantum Dots: Synthesis and Characterization of a Size Series of Highly Luminescent Nanocrystallites. *J. Phys. Chem. B* **1997**, *101*, 9463–9475.
15. Garcia-Santamaria, F.; Brovelli, S.; Viswanatha, R.; Hollingsworth, J. A.; Htoon, H.; Crooker, S. A.; Klimov, V. I. Breakdown of Volume Scaling in Auger Recombination in CdSe/CdS Heteronanocrystals: The Role of the Core−Shell Interface. *Nano Lett.* **2011**, *11*, 687–693.
16. Garcia-Santamaria, F.; Chen, Y.; Vela, J.; Schaller, R. D.; Hollingsworth, J. A.; Klimov, V. I. Suppressed Auger Recombination in "Giant" Nanocrystals Boosts Optical Gain Performance. *Nano Lett.* **2009**, *9*, 3482–3488.
17. Wang, X. Y.; Ren, X. F.; Kahen, K.; Hahn, M. A.; Rajeswaran, M.; Maccagnano-Zacher, S.; Silcox, J.; Cragg, G. E.; Efros, A. L.; Krauss, T. D. Non-blinking Semiconductor Nanocrystals. *Nature* **2009**, *459*, 686–689.
18. Park, Y.-S.; Bae, W. K.; Padilha, L. A.; Pietryga, J. M.; Klimov, V. I. Effect of the Core/Shell Interface on Auger Recombination Evaluated by Single-Quantum-Dot Spectroscopy. *Nano Lett.* **2014**, *14*, 396–402.
19. Cragg, G. E.; Efros, A. L. Suppression of Auger Processes in Confined Structures. *Nano Lett.* **2010**, *10*, 313–317.
20. Kern, S. J.; Sahu, K.; Berg, M. A. Heterogeneity of the Electron-Trapping Kinetics in CdSe Nanoparticles. *Nano Lett.* **2011**, *11*, 3493–3498.
21. Jones, M.; Lo, S. S.; Scholes, G. D. Signatures of Exciton Dynamics and Carrier Trapping in the Time-Resolved Photoluminescence of Colloidal CdSe Nanocrystals. *J. Phys. Chem. C* **2009**, *113*, 18632–18642.
22. McArthur, E. A.; Morris-Cohen, A. J.; Knowles, K. E.; Weiss, E. A. Charge Carrier Resolved Relaxation of the First Excitonic State in CdSe Quantum Dots Probed with Near-Infrared Transient Absorption Spectroscopy. *J. Phys. Chem. B* **2010**, *114*, 14514–14520.
23. Knowles, K. E.; McArthur, E. A.; Weiss, E. A. A Multi-Timescale Map of Radiative and Nonradiative Decay Pathways for Excitons in CdSe Quantum Dots. *ACS Nano* **2011**, *5*, 2026–2035.
24. Garrett, M. D.; Dukes, A. D.; McBride, J. R.; Smith, N. J.; Pennycook, S. J.; Rosenthal, S. J. Band Edge Recombination in CdSe, CdS and CdS_xSe_{1-x} Alloy Nanocrystals Observed by Ultrafast Fluorescence Upconversion: The Effect of Surface Trap States. *J. Phys. Chem. C* **2008**, *112*, 12736–12746.
25. Harrison, M. A.; Ng, A.; Hmelo, A. B.; Rosenthal, S. J. CdSSe Nanocrystals with Induced Chemical Composition Gradients. *Isr. J. Chem.* **2012**, *52*, 1063–1072.

26. Gupta, S.; Kershaw, S. V.; Rogach, A. L. 25th Anniversary Article: Ion Exchange in Colloidal Nanocrystals. *Adv. Mater.* **2013**, *25*, 6923–6943.
27. Swafford, L. A.; Weigand, L. A.; Bowers, M. J., II; McBride, J. R.; Rapaport, J. L.; Watt, T. L.; Dixit, S. K.; Feldman, L. C.; Rosenthal, S. J. Homogeneously Alloyed CdS_xSe_{1-x} Nanocrystals: Synthesis, Characterization, and Composition/Size-Dependent Band Gap. *J. Am. Chem. Soc.* **2006**, *128*, 12299–12306.
28. Logunov, S.; Green, T.; Marguet, S.; El-Sayed, M. A. Interfacial Carrier Dynamics of CdS Nanoparticles. *J. Phys. Chem. A* **1998**, *102*, 5652–5658.
29. Klimov, V.; Bolivar, P. H.; Kurz, H. Ultrafast Carrier Dynamics in Semiconductor Quantum Dots. *Phys. Rev. B* **1996**, *53*, 1463–1467.
30. Pandey, A.; Guyot-Sionnest, P. Intraband Spectroscopy and Band Offsets of Colloidal II–VI Core/Shell Structures. *J. Chem. Phys.* **2007**, *127*, 104710.
31. Rosenthal, S. J.; Xie, X.; Du, M.; Fleming, G. R. Femtosecond Solvation Dynamics in Acetonitrile: Observation of the Inertial Contribution to the Solvent Response. *J. Chem. Phys.* **1991**, *95*, 4715–4718.
32. Rosenthal, S. J.; Jimenez, R.; Fleming, G. R.; Kumar, P. V.; Maroncelli, M. Solvation Dynamics in Methanol: Experimental and Molecular Dynamics Simulation Studies. *J. Mol. Liq.* **1994**, *60*, 25–56.
33. Ekimov, A. I.; Hache, F.; Schanneklein, M. C.; Ricard, D.; Flytzanis, C.; Kudryavtsev, I. A.; Yazeva, T. V.; Rodina, A. V.; Efros, A. L. Absorption and Intensity-Dependent Photoluminescence Measurements on CdSe Quantum Dots: Assignment of the 1st Electronic Transitions. *J. Opt. Chem. Soc. Am. B* **1993**, *10*, 100–107.
34. Scholes, G. D.; Rumbles, G. Excitons in Nanoscale Systems. *Nat. Mater.* **2006**, *5*, 683–696.
35. Klimov, V. I. Spectral and Dynamical Properties of Multiexcitons in Semiconductor Nanocrystals. *Annu. Rev. Phys. Chem.* **2007**, *58*, 635–673.
36. Kambhampati, P. Hot Exciton Relaxation Dynamics in Semiconductor Quantum Dots: Radiationless Transitions on the Nanoscale. *J. Phys. Chem. C* **2011**, *115*, 22089–22109.
37. Allen, M. W. *Measurement of Fluorescence Quantum Yields*; Thermo Fisher Scientific:: Waltham, MA, 2010.
38. Jones, G.; Rahman, M. A. Fluorescence Properties of Coumarin Laser-Dyes in Aqueous Polymer Media: Chromophore Isolation in Poly(methacrylic acid) Hypercoils. *J. Phys. Chem.* **1994**, *98*, 13028–13037.
39. Baumler, W.; Penzkofer, A. Fluorescence Spectroscopic Analysis of n and p Isomers of DODCI. *Chem. Phys.* **1990**, *140*, 75–97.
40. Beaumont, P. C.; Johnson, D. G.; Parsons, B. J. Laser Flash Photolysis Studies of Some Rhodamine Dyes: Characterisation of the Lowest Excited Singlet State of Rhodamine 3B, Sulforhodamine B and Sulforhodamine 101. *J. Chem. Soc., Faraday Trans.* **1998**, *94*, 195–199.
41. Bhasikuttan, A. C.; Suzuki, M.; Nakashima, S.; Okada, T. Ultrafast Fluorescence Detection in Tris(2,2′-bipyridine)-ruthenium(II) Complex in Solution: Relaxation Dynamics Involving Higher Excited States. *J. Am. Chem. Soc.* **2002**, *124*, 8398–8405.